THE JOURNAL OF PHYSICAL CHEMISTRY C

Article

pubs.acs.org/JPCC

Oscillatory Melting Temperature of Stockmayer Fluid in Slit Pores

Chandan K. Das and Jayant K. Singh*

Department of Chemical Engineering, Indian Institute of Technology Kanpur, Kanpur 208016, India

ABSTRACT: The melting transition of bulk and confined Stockmayer fluids (μ^2 = 1) is analyzed using molecular dynamic simulations. The solid−liquid coexistence temperature is evaluated using a modified three-stage pseudo-supercritical transformation path. The bulk melting temperature calculated using the aforementioned method agrees well with the literature value. Melting temperatures of the Stockmayer fluid confined in Lennard-Jones (LJ) 9−3 slit pore of pore size, H, varying from 6 to 20 molecular diameters are reported. For $H \leq 12$ molecular diameters, the shift in the melting temperature for the Stockmayer fluid is oscillatory in nature with the inverse of the pore size. However, for higher H the shift in melting temperature obeys the Gibbs−Thomson equation. The thermodynamic melting temperatures of the Stockmayer fluid under confinement, for variable pore sizes, are found to be usually higher than that of the bulk fluid. The structural and orientational order parameters are also presented, which suggest similarity in the structures of confined LJ and confined Stockmayer fluids.

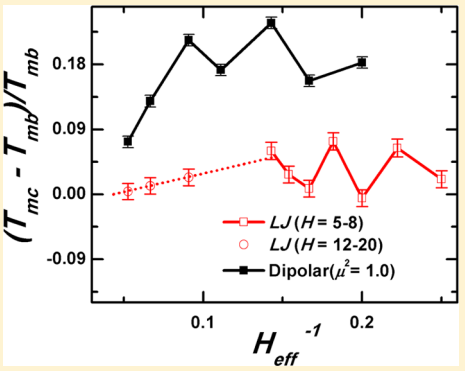

1. INTRODUCTION

Fluids with dipolar interactions are abundant in nature and industry. Ferrofluids (FFs), magnetorheological (MR) fluids, electrorheological (ER) fluids, and polar fluids[1−3] such as water, methanol, chloroform, acetonitrile, aniline, nitrobenzene are the most commonly found dipolar fluids. The magnetic and electric properties of dipolar fluids find widespread application in various fields.[4−6] Numerous theoretical works have described the structures and phase behavior of dipolar fluids.[7−14]

The Stockmayer model is a representative model of dipolar fluids that consists of a short-range Lennard-Jones (LJ) interaction and a long-range anisotropic dipole−dipole interaction. The vapor−liquid thermodynamic properties of the dipolar fluids, such as phase equilibria and interfacial properties, have been demonstrated by earlier workers,[15,16] while few studies have reported on the freezing transition.[17−19] Most of the molecular simulation works on dipolar fluids, until date, have dealt with vapor−liquid systems. Studies on solid−liquid thermodynamics properties for dipolar systems are scarce. Recently, the solid−liquid interfacial properties of Stockmayer fluids have been presented using the cleaving wall method.[20−22] Further, the freezing temperature of Stockmayer fluid is evaluated, for different dipole moments, based on the potential energy discontinuity method by Wang et al.[20] The authors employed the maximum superheating and undercooling technique originally proposed by Luo et al.[23] Most of the work on the dipolar system pertains to the bulk phase. Comparatively, the effect of confinement on the solid−liquid transition of dipolar fluids has not been studied much, particularly using molecular simulation.[24]

Understanding the properties of nanoconfined dipolar fluids is of immense importance in various areas related to lubrication, microfluidics, adhesion, fabrication of nanomaterials, and nanotribology. Hence, numerous experiments have been performed on the phase transitions of confined dipolar fluids. For example, the surface-induced phase-transition of dipolar polystyrene confined between mica surfaces, from liquid-like to solid-like, by reducing the wall separation has been investigated by Klein et al.[25−27] using surface force apparatus. The melting/freezing transition for a strongly dipolar fluid, such as nitrobenzene confined in CPG of different pore sizes, has also been examined recently using differential scanning calorimetric (DSC) and dielectric relaxation spectroscopy by Sliwinska-Bartkowiak et al.[28]

In most of the cases, previous workers have employed density functional theory,[29−31] perturbation theory,[32] or a hysteresis method[20,23] to compute the solid−liquid transition point of dipolar systems. Recently, independent methods have been proposed for the determination of freezing temperature of dipolar fluids, namely the superheating-undercooling method (hysteresis method) and the coexistence solid−liquid method in the NPT and NPH ensembles.[20] Previously, Dominguez and co-workers estimated the free energy of the LJ liquid and solid phases under confinement in order to find the melting point. The authors adopted a method to evaluate the free energy by thermodynamic integration where the wall−fluid interaction was turned off along a thermodynamic path. However, the authors have reported difficulty in finding a reversible thermodynamic path for moderately or strongly attractive walls.[19] Hence, the method adopted by the authors was found to be suitable only for weakly attractive walls. In our recent works, we have avoided the procedure of turning off the wall−

Received: March 27, 2014
Revised: August 20, 2014
Published: August 22, 2014

   dx.doi.org/10.1021/jp503044v | J. Phys. Chem. C 2014, 118, 20848−20857

fluid interaction to find the absolute free energy of the confined phases. Instead, we implemented the three-stage pseudo-supercritical path, along with the multiple histogram reweighting (MHR) technique, for the determination of the Gibbs free energy difference of confined solid and liquid phases to evaluate the melting temperature of LJ systems in slit[33] and cylindrical pores.[34]

In this work, we extend the aforementioned method for Stockmayer fluids to achieve a better understanding of the melting transition of Stockmayer fluids under confinement and to investigate the relation between the pore size and the shift in the melting temperature of a confined dipolar fluid. The rest of the article is structured as follows. The model and method are described in section 2. Section 3 presents the simulation details, and in section 4 the results are presented and discussed. Finally, concluding remarks are presented in section 5.

2. MODEL AND METHODS

2.1. Potential Model. The dipolar fluids are represented by the Stockmayer potential that consists of Lennard-Jones potential along with a pointlike permanent dipole. The potential model, for the fluid−fluid interaction, is given by

$$U_{SM} = U_{ff}^{tr-sh} + U_{dd} \tag{1}$$

where

$$U_{ff}^{tr-sh} = U_{ff}^{lj}(r) - U_{ff}^{lj}(r_c)$$

$$U_{ff}^{lj}(r) = 4\varepsilon_{ff}\left[\left(\frac{\sigma_{ff}}{r}\right)^{12} - \left(\frac{\sigma_{ff}}{r}\right)^{6}\right]$$

$$U_{dd} = \frac{1}{r_{ij}^3}\left[\overline{\mu}_i\cdot\overline{\mu}_i - \frac{1}{r_{ij}^2}(\overline{\mu}_i\cdot r_{ij})(\overline{\mu}_i\cdot r_{ij})\right]$$

where σ_{ff} is the particle diameter, ε_{ff} is the interaction well depth, and r is the distance between two particles. $\overline{\mu}_i$ is the dipole moment of ith particle, and $\overline{r}_{ij}$ denotes the vector connecting the ith and jth particles. All quantities are reduced with respect to ε_{ff} and σ_{ff}. The cutoff radius, r_c, is fixed at $2.6\sigma_{ff}$. The dipole−dipole long-range interaction is treated using the Ewald summation technique.[35,36] We have kept the dipole moment, in this work, fixed at $\mu^2 = 1$.

In this work, the interaction between the structureless wall and a fluid particle at distance z is defined by the LJ9-3 potential.[37] The potential form is as follows

$$U_{wf}(z) = \frac{2}{3}\pi\rho_w\varepsilon_{wf}\sigma_{wf}^3\left[\frac{2}{15}\left(\frac{\sigma_{wf}}{z}\right)^9 - \left(\frac{\sigma_{wf}}{z}\right)^3\right] \tag{2}$$

where ρ_w is the number density of atoms in the wall, and the subscripts f and w represent fluid and wall, respectively. σ_{wf} and ε_{wf} are the cross parameters for the wall−fluid interaction. In this work, we fix $\sigma_{ff} = 1$, $\varepsilon_{ff} = 1$, $\sigma_{ww} = 0.8924$, $\varepsilon_{ww} = 0.1891$, $\rho_w = 6.3049$, $\sigma_{wf} = (\sigma_{ff} + \sigma_{ww})/2$ and $\varepsilon_{wf} = (\varepsilon_{ff}\varepsilon_{ww})^{0.5}$. The strength of interaction of the wall−fluid relative to the fluid−fluid interaction is defined by the coefficient $\alpha = \rho_w\varepsilon_{wf}\sigma^3_{wf}/\varepsilon_{ff}$, which is fixed at 2.32. The slit pore width, H, is varied from 6 to 20 molecular diameters. The cut-off radius for the wall−fluid interaction is fixed at $5\sigma_{ff}$. In this work, all quantities are reduced with respect to σ_{ff} and ε_{ff}.

For a particular pore width, H, the total potential energy is given by

$$\varphi_{pore} = \sum_{i=1}^{N}[\varphi_{fw}(z_i) + \varphi_{fw}(H - z_i)] \tag{3}$$

where, z_i is the distance of a molecule perpendicular to a pore wall, H is the distance between the two pore walls, and N is the number of particles.

2.2. Simulation Methodologies. In this work, we adopt an approach based on the free energy analysis to determine the solid−liquid coexistence of the Stockmayer fluid, which consists of four steps: (a) estimation of the approximate melting point from density−temperature hysteresis curve; (b) computation of equation of state for the solid and liquid phases using the multiple histogram reweighting method at a reference state point; (c) determination of difference in the free energy between solid and liquid phases at an approximate melting temperature using the pseudo-supercritical transformation path; (d) evaluation of the melting temperature is done using the steps (b) and (c), where Gibbs free energy is zero. Each step is described in detail elsewhere;[33,38] however, for completeness we provide a brief summary below.

2.2.1. Estimation of an Approximate Melting Point. At first, solid and liquid phases independently are heated and quenched, respectively, using an isothermal−isobaric ensemble, NP_{xx} (= P_{yy})HT, at $P_{xx} = P_{yy} = 1.0$. The density of the liquid phase gradually increases during the cooling cycle, and at a certain temperature the density rises sharply. In case of the heating cycle, the density decreases gradually at the initial stage, and at a particular temperature it drops sharply. An approximate melting temperature is located within the hysteresis loop.

2.2.2. Solid and Liquid Equation of State. The aim of this step is to construct the Gibbs free energy curves as a function of temperature for both the solid and liquid phases at a constant pressure. The melting temperature is evaluated at which the Gibbs free energy difference between the two phases is zero. The major trouble lies in the calculation of the absolute free energy, which cannot be measured directly from molecular simulation. However, the derivative of the free energy can be estimated with respect to temperature or pressure, which can be integrated to produce the free energy of the system. These curves of free energy plus an unknown constant will be referred to as pure-phase relative free energy curves, since the constant of integration acts as a reference state. The reference state is specific for the given phase.

The selection of temperature range for generation of the free energy curves should be over a small temperature range around the hysteresis loop region. This is performed using the multiple histogram reweighting (MHR) technique of Ferrenberg and Swendsen,[39,40] as elucidated elsewhere.[39−44] The complete detail of its implementation for slit pores can be found in ref 33.

In this work, we perform two separate sets of simulations for the liquid and solid phases. The free energy curves for liquid and solid phases are constructed from histograms, with respect to different reference state points. With the help of free energy difference between the two phases at the approximate melting temperature, the pure phase relative free energy curves can be converted to a solid−liquid free energy difference as a function of temperature. The curves allow estimation of the temperature where free energy is equal for both the solid and liquid phases.

2.2.3. Determination of the Solid−Liquid Free Energy Difference at the Approximate Melting Temperature. The estimation of Helmholtz free energy difference between the

dx.doi.org/10.1021/jp503044v | J. Phys. Chem. C 2014, 118, 20848−20857

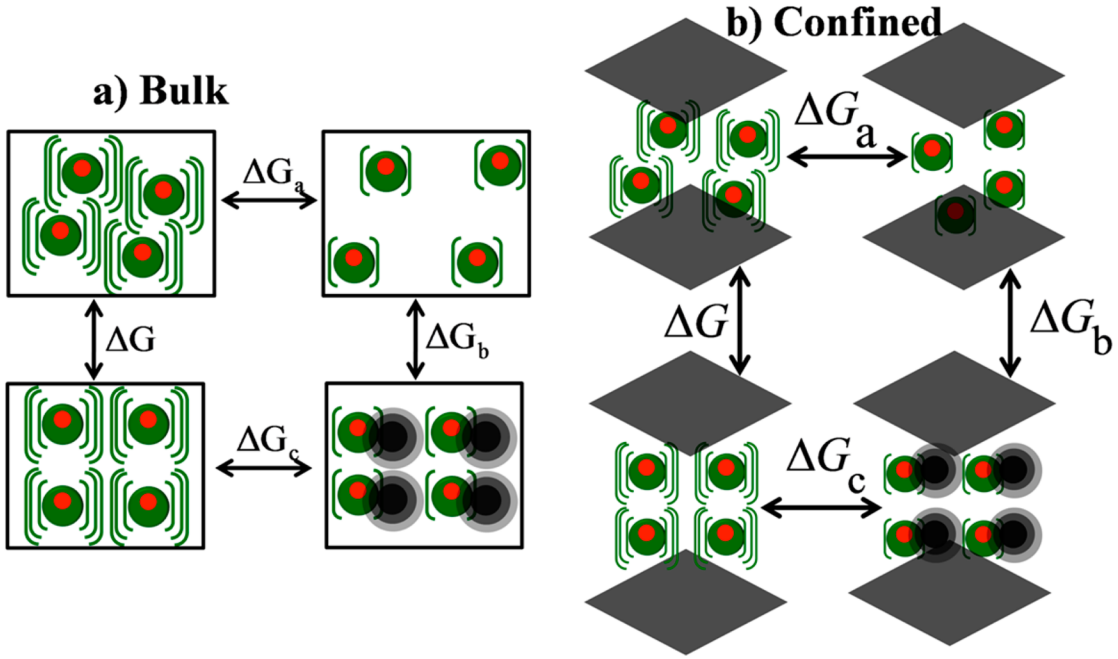

Figure 1. Schematic representation of the three-step pseudo-supercritical transformation path for the bulk (panel a) and confined system (panel b). Red spot on the particle indicates randomly oriented resultant dipole moment. Stage a: the liquid phase is converted to a weakly interacting fluid by gradually reducing the intermolecular interactions and dipole−dipole interaction. Stage b: the Gaussian potential wells are turned on while the volume is reduced to produce a weakly interacting ordered phase. Stage c: the Gaussian wells are turned off while simultaneously intermolecular interactions and dipole−dipole interactions are gradually restored to achieve a crystalline phase.

solid and liquid phases, at an approximate melting temperature, was conducted according to a modified form of the three-stage pseudo-supercritical thermodynamic transformation path.[45] The transformation method was developed on the basis of a reversible thermodynamic path construction between the solid and liquid phases through one or more intermediate states. In order to compute the free energy along the pseudo-supercritical path, a standard thermodynamic integration procedure was used. The fundamental equation for thermodynamic integration is

$$\Delta A^{ex} = \int \left\langle \frac{dU}{d\lambda} \right\rangle_{NVT\lambda} d\lambda \tag{4}$$

where ΔA^{ex} is the difference in the excess Helmholtz free energy and λ is the integration path variable. $\langle dU/d\lambda \rangle_{NVT\lambda}$ indicates the NVT ensemble average for a particular value of λ. Typically, λ is varied from 0 to 1 with $\lambda = 0$ state acting as a reference state. The Helmholtz free energy can be converted to the Gibbs free energy by the addition of a pressure−volume term. The volume changes throughout the three-stage transformation path. In order to estimate the free energy difference between solid and liquid phases, the phases are connected through one or more intermediate states without the first-order phase transition among them. Figure 1 represents the schematic diagram of three-stage pseudo-supercritical path for bulk and confined systems. Though the pseudo-supercritical transformation pathway is described in our earlier work,[33] the three-stage method is briefly described here for better clarity of the work.

2.2.3.1. Stage a. The goal of first step of the pseudo-supercritical path is the conversion of fully interacting liquid to weakly interacting fluid. This is accomplished through a coupling parameter λ, which scales intermolecular interactions in the following manner

$$U_a(\lambda) = [1 - \lambda(1 - \eta)](U_{inter}(r^N) + U_{dd}(r^N, \mu^N)) + \varphi_{fw} \tag{5}$$

where $U_{inter}(r^N)$ is the intermolecular potential energy based on the positions of all N particles, $U_{dd}(r^N,\mu^N)$ is the potential energy due to the long-range dipole−dipole interaction. φ_{fw} represents potential energy due to the wall−fluid interaction which is independent of coupling parameter, and η is a scaling parameter such that $0 < \eta < 1$. The derivative of this function is given by

$$\frac{\partial U_a}{\partial \lambda} = -(1 - \eta)(U_{inter}(r^N) + U_{dd}(r^N, \mu^N)) \tag{6}$$

2.2.3.2. Stage b. In the second stage, the simulation box volume is decreased from the liquid volume to the solid volume. To bring back the liquid particles to the lattice points corresponding to the solid phase, Gaussian attractive potential wells are introduced. These wells are situated at the lattice points of the crystalline phase. The box dimensions along the nonconfined dimensions (L_z) of the liquid and solid phases must be known, either from the MHR results or from isothermal−isobaric simulation runs, at the apparent melting temperature. This ensures that the liquid- and solid-phase pressures are equal at the beginning of stage a and at the end of the transformation path. The potential energy based on λ for this stage is

$$U_b(\lambda) = \eta(U_{inter}[r^N(\lambda)] + U_{dd}[r^N(\lambda), \mu^N]) + \lambda U_{Gauss}[r^N, (\lambda), r_{well}^N(\lambda)] + \varphi_{fw} \tag{7}$$

where, $r^N(\lambda)$ and $r_{well}{}^N(\lambda)$ are the Cartesian coordinates of the particles and potential wells, respectively, which is a function of λ due to the changing box volume. U_{Gauss} represents the potential energy due to the interaction between Gaussian

dx.doi.org/10.1021/jp503044v | J. Phys. Chem. C 2014, 118, 20848−20857

potential wells and particles. The box dimension is modified from the solid volume to the liquid volume, as per the procedure described in our earlier work.[33]

2.2.3.3. Stage c. This is the final stage of the pseudo-supercritical transformation path where the Gaussian potential wells are removed. The potential energy function of this final stage as a function of λ is

$$U_c(\lambda) = [\eta + (1-\eta)\lambda](U_{inter}(r^N) + U_{dd}(r^N, \mu^N)) + (1-\lambda)U_{Gauss}[r^N, r^N_{well}] + \varphi_{fw} \quad (8)$$

and the derivative is given by

$$\frac{\partial U_c}{\partial \lambda} = (1-\eta)[U_{inter}(r^N) + U_{dd}(r^N, \mu^N)] - U_{Gauss}(r^N, r^N_{well}) \quad (9)$$

2.2.4. Finding the Temperature Where ΔG Is Zero. The difference in the excess Helmholtz free energy of solid and liquid phases, $A_s - A_l = \Delta A^{ex} = -(\Delta A_a + \Delta A_b + \Delta A_c)$ can be converted to the Gibbs free energy difference $\Delta G = \Delta A^{ex} + \Delta A^{id} + P\Delta V$, using a simple correlation as mentioned in our earlier work.[33] Here, ΔA_a, ΔA_b, and ΔA_c are the corresponding Helmholtz free energy changes along the stages a, b, and c, respectively. Additionally, the histogram reweighting analysis yields two free energy curves. These free energy curves are used to determine the free energy difference between solid and liquid phases over a small range of temperatures. These curves are also converted with respect to a single reference state point.[33] Finally, the melting temperature is determined where the Gibbs free energy difference is zero.

3. SIMULATION DETAILS

In this work, molecular dynamics simulations are performed using LAMMPS.[46] The velocity−verlet algorithm is used to integrate the equation of motion. The reduced time step is fixed to 0.004. The temperature and pressure are controlled using a Nosé−Hoover thermostat and Anderson barostat,[47] with relaxation time steps of 8×10^3 and 2×10^4 for temperature and pressure, respectively. H is varied from 6 to 20 molecular diameters. Approximately 4600−15000 particles are used to run the simulations. The periodic boundary condition is employed in the X and Y directions of the pore. The pressures along the periodic dimensions are kept fixed. The volume of the confined fluid, for the calculation of densities, is evaluated on the basis of the effective Z dimension: $V = (L_z - \sigma_{wf})L_xL_y$.

First, an approximate melting temperature, T_{am}, is determined by performing two different types of NP_{xx} $(=P_{xx})$ HT simulations. The cooling and heating simulations are performed in a step-by-step procedure after each 3.0×10^6 MD time step with Δt of 0.004 in reduced unit (τ), which is defined as $t(\varepsilon/m\sigma^2)^{1/2}$. In the case of cooling simulations, T is gradually reduced in steps of 0.025 from 1.2 to 0.3, whereas T is increased in steps of 0.025 from 0.3, for heating simulations, until the solid completely loses its crystallinity. The error in the density is estimated using the block averaging method. The histograms for MHR are collected from molecular dynamics simulations at various temperatures. The temperature is chosen according to the following relationship

$$T_i = T_{am} + \sum_{n=-4}^{4} n\Delta T$$

where T_{am} is the approximate melting temperature estimated from the hysteresis data; ΔT is chosen in accordance with the metastable region. At each temperature an equilibration run of 2×10^5 MD steps is performed followed by a production run of 3×10^6 MD steps.

The thermodynamic integration calculations along the three-stage pseudo-supercritical path are conducted using NVT molecular dynamics. For each integration stage, 10 simulations are conducted, with the values of λ chosen according to the standard 10-point Gauss−Legendre integration scheme. The Gaussian potential well parameters are taken from the work of Grochola.[38,45]

At the first stage of the transformation path, simulations are started from a random initial configuration (i.e., $\lambda = 0$), which is obtained during the hysteresis runs. Subsequently, each λ initial configuration is taken from its previous λ simulation, and the total time steps for each λ is 5×10^6. For the second stage, stage b, the last configuration of the stage a is used as the initial configuration. However, to obtain the final configuration we put dummy atoms on the crystal lattice point obtained from the heating run. The Gaussian potential wells are attached to these dummy atoms. The simulation box dimensions L_x and L_y are reduced accordingly to λ values which are already derived in our earlier work.[33] The initial configuration for the third stage is taken from the heating run of hysteresis loop at T_{am}, and the dummy atoms are created as described for the second stage. Separate sets of simulations are conducted as per Eike et al.[38] to determine the thermodynamic melting temperature of the bulk dipolar fluid at $P = 0$ and $P = 1$. The error in the melting temperature is calculated from the propagation of error method associated with the value of integrand. The error in integrand is calculated using the block averaging method.

4. RESULTS AND DISCUSSION

4.1. Bulk Stockmayer Fluid. We start our discussion with the bulk Stockmayer fluid at $P = 0$. Figure 2 shows a plot of the density as a function of the temperature for both the quenching and heating cases. As the liquid is quenched, the density gradually increases and at a certain temperature the density rises sharply. In case of a heating run of the solid phase, the

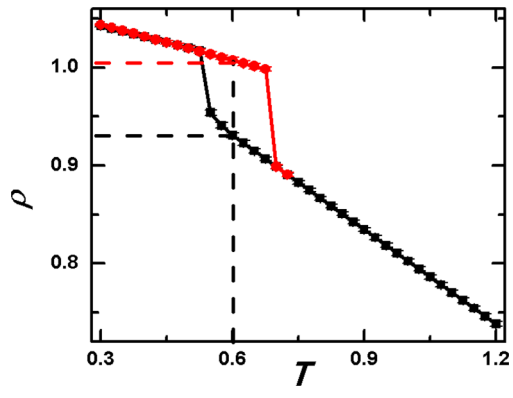

Figure 2. Density as a function of temperature for solid and liquid phases at zero pressure. Symbols square and circle represent quenching and heating cycles, respectively. The solid (top curve) progressively heated from $T = 0.3$ to 0.725 until complete loss of crystallanity, while the liquid (bottom) is quenched progressively from $T = 1.2$ to 0.3. Vertical dash line indicates an approximate melting temperature(T_{am}). Horizontal dash lines indicate corresponding densities of solid and liquid at T_{am}.

dx.doi.org/10.1021/jp503044v | J. Phys. Chem. C 2014, 118, 20848−20857

density decreases and at a particular temperature the density drops sharply. The hysteresis loop, as shown in Figure 2, indicates a first-order phase transition. A wide metastable region is observed around the true phase-transition point. The true melting point is adjacent to the metastable region. Figure 2 clearly shows that abrupt density change or a discontinuous drop in density occurs at $T = 0.70$, which indicates that the true thermodynamic melting temperature would be lower than this temperature. In Figure 2, the vertical dashed line represents the approximate melting temperature $T_{am} = 0.60$, at which the free energy difference between solid and liquid phases is evaluated using the pseudo-supercritical transformation path. The solid and liquid box lengths are determined from the corresponding densities as shown by the horizontal dotted lines.

The Gibbs free energy curves are constructed taking $T = 0.60$ as an intermediate point of the metastable region. As described in the methodology section, simulations are performed at nine different temperatures. For each temperature, two sets of simulations are performed: one for the heating case and another one for the quenching case, resulting in 18 histograms. The relative Gibbs free energy curves for both phases are generated independently by collecting the histograms for the solid and the liquid phases. The Gibbs free energy curves are constructed with respect to the lowest temperature state point for each phase. Figure 3 presents the Gibbs free energy curves

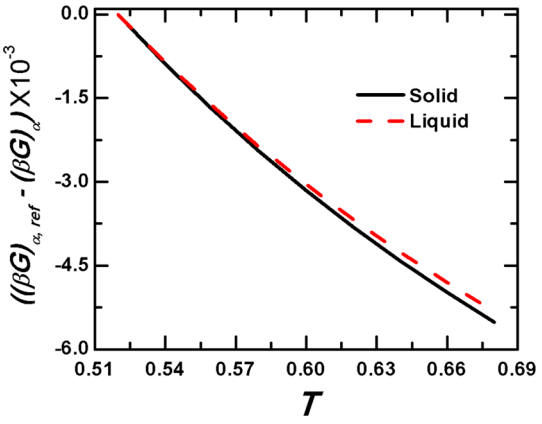

Figure 3. Relative Gibbs free energy curves as a function of temperature for bulk dipolar fluid at zero pressure relative to their respective reference state, constructed from MHR.

for the solid and the liquid phases with respect to their respective reference state. The next step is the evaluation of the Gibbs free energy difference between the two phases at an approximate melting temperature.[33]

The thermodynamic integration is performed at T_{am} along the pseudo-supercritical path, through which solid and liquid phases are connected avoiding the first-order phase transition (see Figure 1). The box lengths for solid and liquid phases are determined from their respective densities as shown by corresponding horizontal lines in Figure 2. The box lengths are chosen in such a way that pressure remains constant at the beginning of the stage-a and at the end of the stage-c.[33] Plots of $\langle \partial U/\partial \lambda \rangle_{NVT\lambda}$ as a function of λ for three stages of thermodynamic integration are shown in Figure 4. Figure 4 shows that curves are continuous and integrable for all the three steps. In the case of the bulk fluid, we have followed the method as per Eike et al.[38] Table 1 summarizes the various contributions to the Gibbs free energy difference.

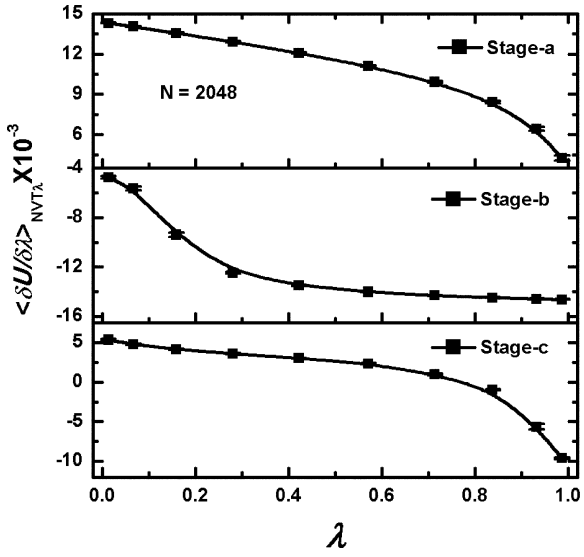

Figure 4. $\langle \partial U/\partial \lambda \rangle_{NVT\lambda}$ as a function of λ for the three-stage pseudo-supercritical transformation path for the bulk dipolar system at zero pressure.

Once the Gibbs free energy difference of two phases is determined at an approximate melting temperature, it is no longer difficult to convert the liquid Gibbs free energy curve relative to a solid reference state as shown in ref 33. The two Gibbs free energy curves with respect to a single reference state point are shown in Figure 5. Using the relative free energy between the crystalline and liquid phases at a single point, the free energy difference between crystalline and liquid phases can be evaluated for all other points. By determining ΔG in this way over a range of temperatures, a ΔG vs temperature curve can be produced, and the temperature where this curve is zero produces a single coexistence point or the thermodynamic melting temperature. The coexistence temperature calculated using the above-mentioned method is 0.660(6).[48] Our calculated value at zero pressure is consistent with that of Wang et al.[20] We have also evaluated the melting temperature of bulk dipolar LJ system at $P = 1$, using the three-stage pseudocritical transformation path along with MHR. The melting temperature obtained at $P = 1$ (see Table 1) is 0.674(5), which is little higher in comparison to the case of zero pressure.

4.2. Stockmayer Fluid in Slit Pore. Now, we turn our attention on the effects of confinement on the melting temperature of a Stockmayer fluid. In our previous note, we have reported the thermodynamics melting temperature of a Lennard-Jones solid in slit pore.[33]The melting temperatures for larger slit pores were found to obey the Gibbs−Thomson equation, $\Delta T_f = T_{f,pore} - T_{f,bulk} = -2[(\gamma_{ws} - \gamma_{ws})\nu/(H\lambda_{f,bulk})]$. Where, the shift in the freezing/melting temperature ΔT_f is related to the inverse of the pore width H; γ_{ws} and γ_{wf} are the wall−solid and wall−fluid surface tensions, ν is the molar volume of the liquid phase, and $\lambda_{f,bulk}$ is the bulk latent heat of melting. Interestingly, for narrow pores the melting temperatures of confined LJ solids were found to be oscillatory in nature. However, it is not yet known if such behavior holds also for complex fluids. In order to address the question, in this work we consider the case of confined Stockmayer fluids. We have chosen a strongly attractive LJ9-3-based slit pore, with a relative wall−fluid strength of $\alpha = 2.32$ as employed in a previous work,[33] for a suitable comparison between the

dx.doi.org/10.1021/jp503044v | J. Phys. Chem. C 2014, 118, 20848−20857

Table 1. Estimated True Thermodynamic Melting Temperature, T_m, and Various Contributions to the Gibbs Free Energy, for Different Pore Sizes, H, with Variable Wall−fluid Interaction Strength at an Approximate Melting Temperature (T_{am})[a]

H	T_{am}	ρ_L	ρ_S	ΔA^{ex}	ΔA^{id}	$P\Delta V$	ΔG	T_m
				bulk μ = 1.0, P = 0				
	0.600	0.931	1.007	−137.9(7)	97.109	0.00	−40.777	0.660(6)
				bulk μ = 1.0, P = 1				
	0.600	0.951	1.009	21.6(2)	72.370	−123.113	−29.144	0.674(5)
				wall (LJ9−3), μ = 1, ε_{wf} = 0.4348, α = 2.32				
20	0.650	0.945	1.008	−111(3)	604.003	−1014832	−522.149	0.724(3)
16	0.675	0.934	1.017	−441.9(22)	583.221	−886.703	−745.457	0.753(3)
12	0.800	0.868	0.976	−43.9(14)	717.996	−43.916	−301.119	0.818(1)
10	0.775	0.901	0.990	−53.0(7)	420.267	−53.079	−205.406	0.790(1)
8	0.800	0.903	1.015	−15.8(8)	523.060	−15.764	−175.966	0.834(1)
7	0.825	0.890	1.027	−39.0(5)	609.560	−773.344	−202.805	0.781(2)
6	0.775	0.931	1.058	90.9(6)	456.137	−593.325	−46.215	0.797(1)

[a]ΔG denotes the Gibbs free energy difference at T_{am}. ρ_L and ρ_S represent corresponding densities of liquid and solid respectively at T_{am}.

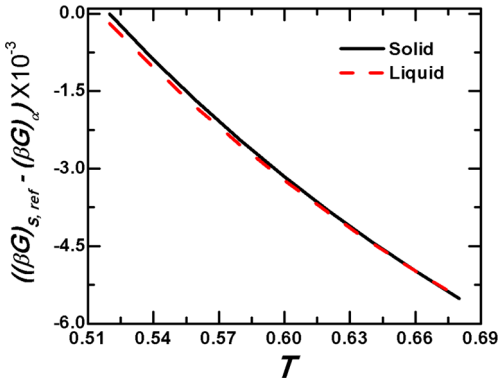

Figure 5. Relative Gibbs free energy as a function of temperature for the bulk dipolar system at zero pressure constructed from MHR. Both branches are relative to the solid reference state.

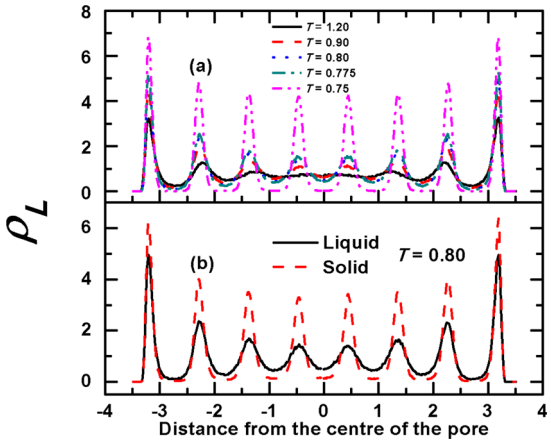

Figure 6. (a) Local density (ρ_L) as a function of pore distance from the center of the pore for H = 8 for the quenching case. (b) Comparison of local density profile for the solid and the liquid phases at T_{am} = 0.80.

Stockmayer fluid and the LJ fluid. Pore size is varied from 6 to 20 molecular diameters. We observe that the determination of melting temperature of dipolar system using kinetic approach is not feasible unlike for Lennard-Jones fluids.[48] Hence, we adopt thermodynamic approach for confined Stockmayer fluids, using the pseudocritical transformation method, to evaluate the solid−liquid coexistence under confinement. As previously mentioned, the first step in evaluating the true thermodynamic melting temperature is to determine an approximate melting temperature. We first calculate the overall density of the confined system along the quenching and heating paths, which shows that at T = 0.85 density drops sharply. Similar to the earlier case, we choose an approximate melting temperature lower than the above value, T_{am} = 0.80.

Figure 6 (a, top) presents the local density for various temperatures during the quenching run. At higher temperatures, the peak heights of the layers are not pronounced. However, with decrease in the temperature the peak-height increases, and sharp distinct peaks are observed at T = 0.75 indicative of the solid phase. From the change in the peak-height and shape, one can distinguish between the solid and liquid phases, and also estimate the melting temperature approximately. Figure 6 (b, bottom) shows the typical density profiles for the solid and liquid phases at T_{am} = 0.80. However, determination of the true thermodynamics melting transition point requires calculation of the free energy for both the solid and liquid phases. We have also examined the corresponding crystal structure under confinement. The observed crystal structures and the plane of orientation are similar to that seen for LJ fluids confined in slit pores.[33] Figure 7 presents the side views and top views of the crystal structures, for various pores widths. As shown in Figure 7, the plane of orientation is akin to the FCC planes, which is also observed for LJ fluids in slit confinement.[33] This is also confirmed by Figure 8, which presents a comparison of crystal structures between confined LJ and dipolar fluids. The structure is more or less unchanged within the range of the pore size considered in this work.

In-plane bond orientational order parameters(ψ_4/ψ_6) are determined as described in our previous work.[33,34] Figure 9 presents the comparison of in-plane bond orientatonal order parameter between LJ and Stockmayer fluids in a slit pore of width, H = 8, as a function of temperature. The ψ_6 values of the confined Stockmayer fluid are always higher than ψ_4 (see Table 2), for all the layers, indicating higher propensity of triangular or hexagonal symmetry in the crystal plane. Interestingly, the inner layer of the confined Stockmayer fluid is well ordered, which is contradictory to that seen for the confined LJ fluids.[49] This is clearly indicated by the order parameter values, which is more or less similar to that of the contact layer or the second layer. On the other hand, ψ_6 values for inner layers of the confined LJ fluid is less in comparison to that of the contact layer, second layer or third layer. For all the cases, crystal structures of confined Stockmayer solids are rich in triangular

dx.doi.org/10.1021/jp503044v | J. Phys. Chem. C 2014, 118, 20848−20857

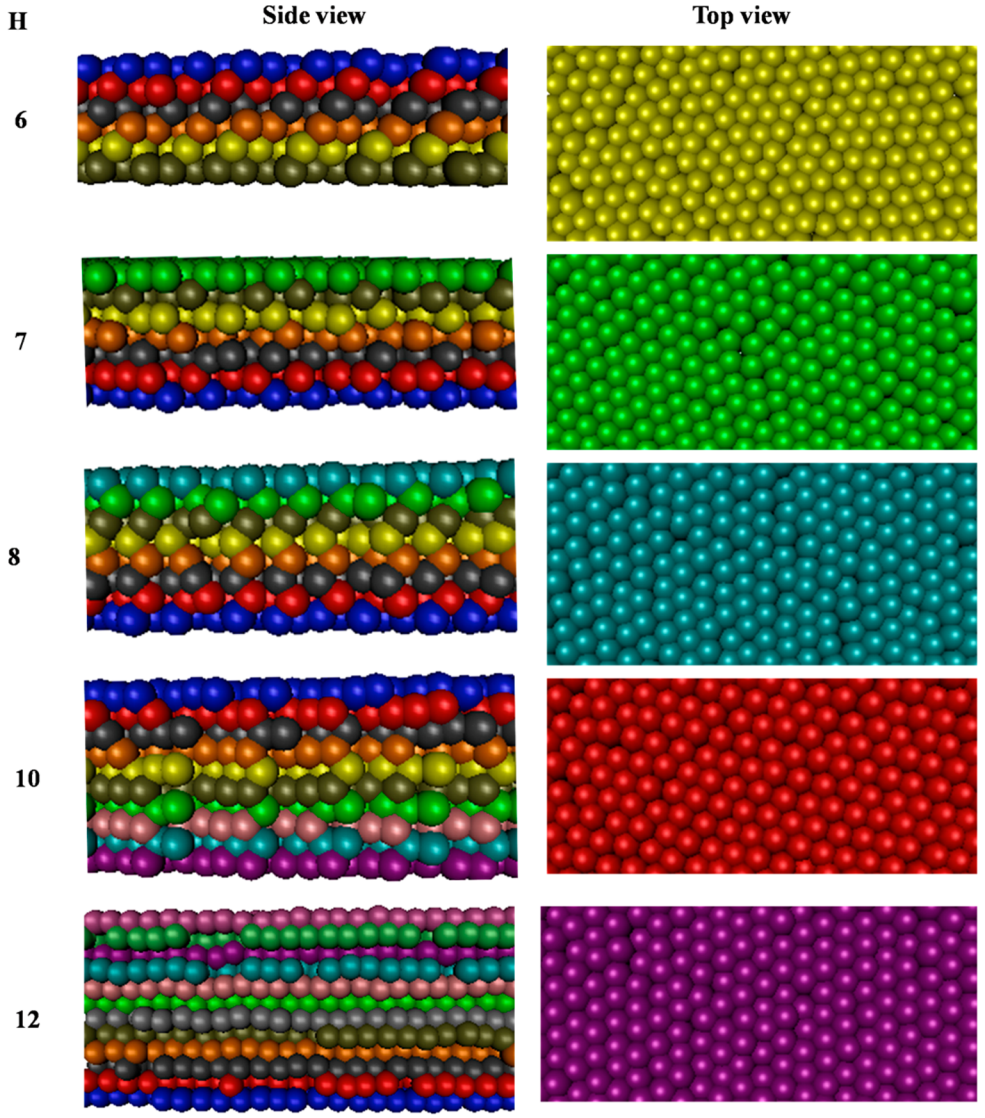

Figure 7. Snapshots of crystal structures (side and top views) of dipolar systems for different pores at $T = 0.70$.

symmetry, which is in-line with that observed for confined LJ solids.[33]For example, for $H = 8$ all the 8 layers have triangular symmetry and is represented by 8T. Though we present values of the contact layer, other layers also follow the same trend. The bond orientational order parameters and the symmetry in the crystal structures for various wall separations are summarized in Table 2. Figure 9 suggests that the generic behavior of all the layers is similar for both confined LJ and Stockmayer fluids. A very steep drop in ψ_6 values, for both the cases, are observed between $T = 0.825$ to 0.85. This behavior suggests that all molecular layers undergo a transition from ordered solid phase to isotropic liquid phase in between $T = 0.825$ and 0.85. Thus, conclusion on true thermodynamic melting temperature based on the bond orientation order parameter is questionable.

In order to determine the true thermodynamic melting temperature of confined dipolar fluid, we have used a combination of Grochola's three stages pseudo-supercritical transformation path and multiple histogram reweighting (MHR) technique. The Gibbs free energy curves are constructed taking $T = 0.80$ as an intermediate point of the metastable region. As described previously, simulations are performed at nine different temperatures, taking approximate melting temperature as the middle/central point of nine simulations. For each temperature, two sets of simulations are performed: one for the heating case and another for the quenching case, resulting in 18 histograms. The relative Gibbs free energy curves for both the phases are generated by collecting the histograms separately for solid and liquid phases. The Gibbs free energy curves are constructed with respect to the lowest temperature state point for each phase similar to that for the bulk case (see Figure 1). The thermodynamic integration is performed at an approximate melting temperature, $T_{am} = 0.80$. The box lengths are chosen in such a way that $P_{xx} = P_{yy} = 1$ remains constant at the beginning of the stage a and at the end of the stage c.[33] Plots of $\langle \partial U/\partial \lambda \rangle_{NVT\lambda}$ as a function of λ for the three stages of thermodynamic integration are continuous and integrable for all the three steps. Further, in this work, we have also checked the reversibility of the considered thermodynamic path. For all three cases, error bars are of the order of symbol size. The different contributions to the Gibbs free energy for all the wall separations are summarized in Table1.

dx.doi.org/10.1021/jp503044v | J. Phys. Chem. C 2014, 118, 20848−20857

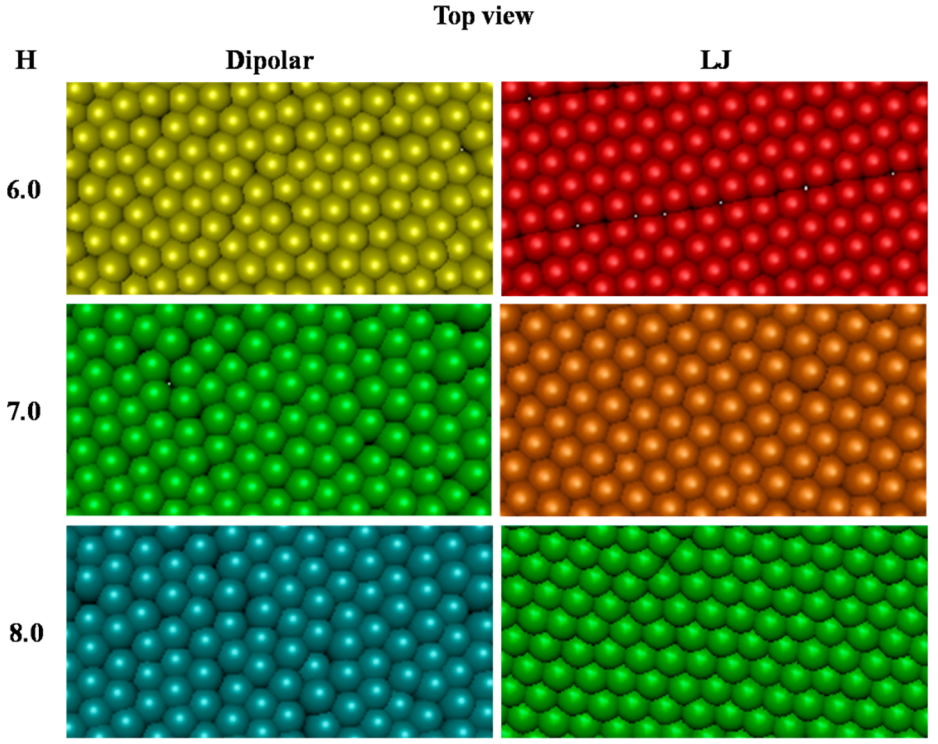

Figure 8. Comparison of in-plane orientation of crystal structures between confined LJ and dipolar fluids (top view).

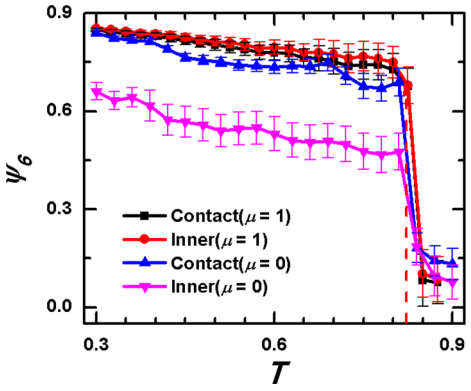

Figure 9. Average in-plane orientational order parameters for Stockmayer and LJ fluids are presented as a function temperature for H = 8. Vertical dashed line indicates sudden drop in ψ_6 at around melting temperature. Error bar is estimated using the block-averaging method.

Table 2. Crystal Structures and Orientation Order Parameters with Wall Separation, Where *nT* Represents *n* Layers in Triangular Symmetry

H	structures	Ψ_4	Ψ_6
6	6T	0.037	0.567
7	7T	0.176	0.426
8	8T	0.201	0.776
10	10T	0.025	0.321
12	12T	0.172	0.842
16	16T	0.056	0.447
20	20T	0.146	0.379

Once the Gibbs free energy difference of two phases is determined at an approximate melting temperature, the Gibbs free energy curve relative to a solid reference state is evaluated as per ref 38. Using the relative free energy between the crystalline and liquid phases at a single point, the free energy difference between crystalline and liquid phases can be evaluated for all other points. By determining ΔG in this way over a range of temperatures, a ΔG vs temperature curve can be produced, and the temperature where ΔG is zero produces a single coexistence point or the thermodynamic melting temperature. In order to assess the system size effect, we simulated a system with 2-fold increase in the cross-section area and the number of particles (N = 12672). However, we do not find any significant change in the melting temperature. The estimated true thermodynamic melting temperatures for different pore sizes are summarized in Table 1. It should be noted that melting temperature of the Stockmayer fluid as calculated in this work is lower than that of the LJ fluid.[33] This primarily is attributed to the lower cut off distance, employed in this work, for the Stockmayer fluid (Rc = $2.6\sigma_{ff}$) compared to that for the LJ fluid (Rc = $5\sigma_{ff}$).

Figure 10 presents a plot of the scaled shift in T_m $[(T_{mc} - T_{mb})/T_{mb}]$ against the inverse of the wall separation, where T_{mb} is the bulk melting temperature and T_{mc} is the melting temperature under confinement. In this work, we have observed an elevation of melting temperature of confined Stockmayer fluid for all the pore sizes studied in this work, as shown in Figure 10. However, there is no specific relationship between the melting temperature and the slit separation. In fact, the melting temperature of the confined Stockmayer fluid is oscillatory in nature, as also found by previous workers via different methods albeit for the Lennard-Jones fluid.[33,48] The elevation in the melting temperature in attractive pores, as seen in this work, is also observed in other studies.[33,50−52] In our previous works,[33,48] we have reported that the kinetic melting temperature displays both elevation and depression behavior with wall separation. Interestingly, in this work we observe only

dx.doi.org/10.1021/jp503044v | J. Phys. Chem. C 2014, 118, 20848−20857

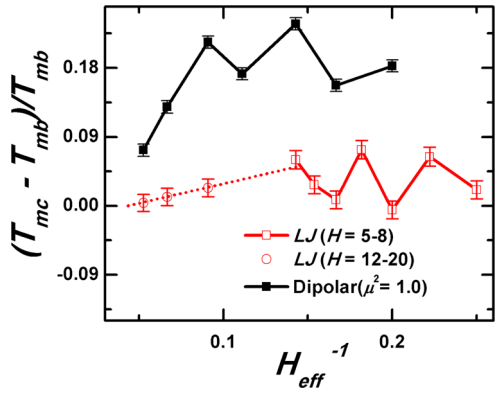

Figure 10. Shift in melting temperature reduced by the bulk melting temperature is presented as a function of inverse of the effective pore size, H. Filled and open symbols represent Stockmayer fluid and LJ fluid, respectively.

elevation in the thermodynamic melting temperature with respect to that of the bulk solid.

It is noted that the oscillatory behavior in the melting temperature is observed for narrow pores, which starts to decay at around pore size of $H = 12$ for the confined Stockmayer fluid. Subsequently, the behavior is linear with the pore size for $H > 12$. The behavior seen in the shift in the melting behavior of the confined dipolar fluid is in line with that observed for the confined LJ fluids. Based on the data, as shown in Figure 10, we expect that the confinement effects will completely disappear at a pore size $H \sim 30$, which is slightly higher than that for LJ fluids ($H \sim 25$) in slit confinement.[33] The oscillatory behavior in the melting temperature seen for Lennard-Jones and Stockmayer fluids[33,48] can be an indicative of a generic behavior of confined solids in narrow pores. However, more work is needed in order to generalize the melting/freezing behavior for confined fluids in narrow pores.

5. CONCLUSION

In this work, we demonstrate the melting behavior of the Stockmayer fluid, with $\mu^2 = 1$, confined in strongly attractive slit pores of different pore sizes in addition to the bulk fluid. The thermodynamic melting temperatures of confined dipolar fluids are evaluated using a pseudo-supercritical transformation path connecting the solid phase and the liquid phase without the first-order phase transition. The method is successfully implemented for dipolar fluids to obtain the solid−liquid coexistence under confinement. The method is computationally intensive as the Ewald summation technique is employed for the long-range dipole−dipole interaction. However, the method employed is advantageous over other existing methods, since separate evaluation of the free energy of each phase is not required. The melting temperature of the bulk solid at $P = 1$ is higher in comparison to that at zero pressure. The melting temperatures of confined Stockmayer solid at lower pore sizes are oscillatory in nature. The oscillatory nature of melting temperature with pore size is confirmed with an accurate estimate of the true melting temperature. However, at higher pores size, $H > 12$, the shift in melting temperature is in line with the prediction of the Gibbs−Thomson equation.

AUTHOR INFORMATION

Corresponding Author

*E-mail: jayantks@iitk.ac.in.

Notes

The authors declare no competing financial interest.

ACKNOWLEDGMENTS

This work was supported by the Department of Science and Technology, Government of India. Computational resources are provided by the HPC cluster of the Computer Center (CC), Indian Institute of Technology Kanpur.

REFERENCES

(1) Leeuwen, M. v. Derivation of Stockmayer Potential Parameters for Polar fluids. *Fluid Phase Equilib.* **1994**, *99*, 1−18.
(2) Halsey, T. C. Electrorheological Fluids. *Science* **1992**, *258*, 761−766.
(3) Halsey, T.; Martin, J. Electrorheological Fluids. *Sci. Am.* **1993**, *269*, 58−64.
(4) Stangroom, J. E. Elentrorheological fluids. *Phys. Technol.* **1983**, *14*, 290−296.
(5) Wen, W.; Wang, N.; Ma, H.; Lin, Z.; Tam, W. Y.; Chan, C. T.; Sheng, P. Field Induced Structural Transition in Mesocrystallites. *Phys. Rev. Lett.* **1999**, *82*, 4248−4251.
(6) Blaaderen, A. v. From the de Broglie to Visible Wavelengths: Photons With Colloids. *MRS Bull.* **1998**, *23*, 39−43.
(7) Klapp, S.; Forstmann, F. Phase Transitions in Dipolar Fluids: An Integral Equation Study. *J. Chem. Phys.* **1997**, *106*, 9742−9761.
(8) Tavares, J. M.; Teixeira, P. I. C. Patching up Dipoles: Can Dipolar Particles be Viewed as Patchy Colloids? *Mol. Phys.* **2011**, *109*, 1077−1085.
(9) Teixeira, P. I. C.; Tavares, J. M.; Gama, M. M. T. d. The Effect of Dipolar Forces on the Structure and Thermodynamics of Classical Fluids. *J. Phys: Condns. Matter* **2000**, *12*, R411−R434.
(10) Osipov, M.; Teixeira, P.; Gama, M. M. T. d. Structure of Strongly Dipolar Fluids at Low Densities. *Phys. Rev. E* **1996**, *54*, 2597−2609.
(11) Teixeira, P. I.; Gama, M. M. T. d. Density-Functional Theory for the Interfacial Properties of a Dipolar Fluid. *J. Phys.: Condens. Matter* **1991**, *3*, 111−125.
(12) Groh, B.; Dietrich, S. Long-Ranged Orientational Order in Dipolar Fluids. *Phys. Rev. Lett.* **1994**, *72*, 2422−2425.
(13) Sear, R. Low-Density Fluid Phase of Dipolar Hard Spheres. *Phys. Rev. Lett.* **1996**, *76*, 2310−2313.
(14) Groh, B.; Dietrich, S. Ferroelectric Phase in Stockmayer Fluids. *Phys. Rev. E* **1994**, *50*, 3814−3833.
(15) Paul, S.; Chandra, A. Liquid-Vapor Interfaces of Simple Electrolyte Solutions: Molecular Dynamics Results for Ions in Stockmayer Fluids. *J. Phys. Chem. B* **2003**, *107*, 12705−12712.
(16) Mecke, M.; Fischer, J.; Winkelmann, J. Molecular Dynamics Simulation of the Liquid−Vapor Interface of Dipolar Fluids Under Different Electrostatic Boundary Conditions. *J. Chem. Phys.* **2001**, *114*, 5842−5852.
(17) Groh, B.; Dietrich, S. Crystal Structures and Freezing of Dipolar Fluids. *Phys. Rev. E* **2001**, *63*, 021203−1−021203−11.
(18) Gao, G. T.; Zeng, X. C. Freezing Transition of a Strongly Dipolar Simple Fluid. *Phys. Rev. E* **2000**, *61*, R2188−R2191.
(19) Dominguez, H.; Allen, M. P.; Evans, R. Monte Carlo studies of the freezing and condensation transitions of confined fluids. *Mol. Phys.* **1999**, *96*, 209−229.
(20) Wang, J.; Apte, P. A.; Morris, J. R.; Zeng, X. C. Freezing Point and Solid-Liquid Interfacial Free Energy of Stockmayer Dipolar Fluids: A Molecular Dynamics Simulation Study. *J. Chem. Phys.* **2013**, *139*, 114705−1−114705−11.
(21) Davidchack, R. L.; Laird, B. B. Direct Calculation of the Crystal−Melt Interfacial Free Energies for Continuous Potentials: Application to the Lennard-Jones System. *J. Chem. Phys.* **2003**, *118*, 7651−7657.
(22) Broughton, J. Q.; Gilmer, G. H. Molecular Dynamics Investigation of the Crystal−Fluid Interface. VI. Excess Surface Free

Energies of Crystal−Liquid Systems. *J. Chem. Phys.* **1986**, *84*, 5759−5768.
(23) Luo, S.-N.; Ahrens, T. J.; ağın, T. C.; Strachan, A.; W. A, G., III; Swift, D. C. Maximum Superheating and Undercooling: Systematics, Molecular Dynamics Simulations, and Dynamic Experiments. *Phys. Rev. B* **2003**, *68*, 134206−1−134206−11.
(24) Froltsov, V. A.; Klapp, S. H. L. Dielectric Response of Polar Liquids in Narrow Slit Pores. *J. Chem. Phys.* **2007**, *126*, 114703−1−114703−10.
(25) Klein, J.; Perahia, D.; Warburg, S. Forces Between Polymers-Bearing Surfaces Undergong Shears. *Nature* **1991**, *352*, 143−145.
(26) Klein, J.; Kumacheva, E.; Perahia, D.; Mahalu, D.; Warburg, S. Interfacial Sliding of Polymer-bearing Surfaces. *Faraday Spec. Discuss. Chem. Soc.* **1994**, *98*, 173−188.
(27) Klein, J.; Kumacheva, E. Confinement-Induced Phase Transitions in Simple Liquids. *Science* **1995**, *269*, 816−819.
(28) Sliwinska-Bartkowiak, M.; Gras, J.; Sikorski, R.; Radhakrishnan, R.; Gelb, L.; Gubbins, K. E. Phase Transitions in Pores: Experimental and Simulation Studies of Melting and Freezing. *Langmuir* **1999**, *15*, 6060−6069.
(29) Groh, B.; Dietrich, S. Density-Functional Theory for the Freezing of Stockmayer Fluids. *Phys. Rev. E* **1996**, *54*, 1687−1697.
(30) Klapp, S.; Forstmann, F. Stability of Ferroelectric Fluid and Solid Phases in the Stockmayer Model. *Europhys. Lett.* **1997**, *38*, 663−668.
(31) B.Warshavsky, V.; Zeng, X. C. Effect of an Electric Field on the Surface Tension of a Dipolar-Quadrupolar Fluid and Its Implication for Sign Preference in Droplet Nucleation. *Phys. Rev. Lett.* **2002**, *89*, 246104−1−246104−4.
(32) Leeuwen, M. E. V.; Smit, B.; Hendriks, E. M. Vapour-Liquid Equilibria of Stockmayer Fluids Computer Simulations and Perturbation Theory. *Mol. Phys.* **1993**, *78*, 271−283.
(33) Das, C. K.; Singh, J. K. Effect of Confinement on the Solid-Liquid Coexistence of Lennard-Jones Fluid. *J. Chem. Phys.* **2013**, *139*, 174706−1−174706−13.
(34) Das, C. K.; Singh, J. K. Melting Transition of Lennard-Jones Fluid in Cylindrical Pores. *J. Chem. Phys.* **2014**, *140*, 204703−1−204703−9.
(35) Toukmaji, A.; Sagui, C.; Board, J.; Darden4, T. Efficient Particle-Mesh Ewald Based Approach to Fixed and Induced Dipolar Interactions. *J. Chem. Phys.* **2000**, *113*, 10913−10926.
(36) Veld, P. J. i. t.; Ismail, A. E.; Grest, G. S. Application of Ewald Summations to Long-Range Dispersion Forces. *J. Chem. Phys.* **2007**, *127*, 144711−1−144711−8.
(37) Alba-Simionesco, C.; Coasne, B.; Dosseh, G.; Dudziak, G.; Gubbins, K. E.; Radhakrishnan, R.; Sliwinska-Bartkowiak, M. Effects of Confinement on Freezing and Melting. *J. Phys.: Condens. Matter* **2006**, *18*, R15−R68.
(38) Eike, D. M.; Brennecke, J. F.; Maginn, E. J. Toward a Robust and General Molecular Simulation Method for Computing Solid-Liquid Coexistence. *J. Chem. Phys.* **2005**, *122*, 014115−1−014115−12.
(39) Ferrenberg, A. M.; Swendsen, R. H. New Monte Carlo Technique for Studying Phase Transitions. *Phys. Rev. Lett.* **1988**, *61*, 2635−2635.
(40) Ferrenberg, A. M.; Swendsen, R. H. Optimized Monte Carlo Data Analysis. *Phys. Rev. Lett.* **1989**, *63*, 1195−1198.
(41) Kiyohara, K.; Gubbins, K. E.; Panagiotopoulos, A. Z. Phase Coexistence Properties of Polarizable Stockmayer Fluids. *J. Chem. Phys.* **1997**, *106*, 3338−3347.
(42) Conrad, P. B.; Pablo, J. J. d. Comparison of Histogram Reweighting Techniques for a Flexible Water Model. *Fluid Phase Equilib.* **1998**, *150−151*, 51−61.
(43) Chang, J.; Sandler, S. I. Determination of Liquid−Solid Transition using Histogram Reweighting Method and Expanded Ensemble Simulations. *J. Chem. Phys.* **2003**, *118*, 8390−8395.
(44) Chang, J.; Lenhoff, A. M.; Sandler, S. I. Determination of Fluid−Solid Transitions in Model Protein Solutions Using the Histogram Reweighting Method and Expanded Ensemble Simulations. *J. Chem. Phys.* **2004**, *120*, 3003−3014.
(45) Grochola, G. Constrained Fluid Lambda-Integration:Construction a Reversible Thermodynamics Path Between the Solid and Liquid State. *J. Chem. Phys.* **2004**, *120*, 2122−2126.
(46) Plimpton, S. J. Fast Parallel Algorithms for Short−Range Molecular Dynamics. *J. Comp. Phys.* **1995**, *117*, 1−19.
(47) Martyna, G. J.; Tuckerman, M. E.; Tobias, D. J.; Klein, M. L. Explicit Reversible Integrators for Extended Systems Dynamics. *Mol. Phys.* **1996**, *87*, 1117−1157.
(48) Das, C. K.; Singh, J. K. Melting Transition of Confined Lennard-Jones Solids in Slit Pores. *Theor. Chem. Acc.* **2013**, *132*, 1351−1−1351−13.
(49) Sliwinska-Bartkowak, M.; Hung, F. R.; Santiso, E. E.; Coasne, B.; Dudziak, G.; Siperstein, F. R.; Gubbins, K. E. Effect of Confinement on Freezing of CCl4 in Cylindrical Pores. *Adsorption* **2005**, *11*, 391−396.
(50) Miyahara, M.; Gubbins, K. E. Freezing/Melting Phenomena for Lennard-Jones Methane in Slit Pores: A Monte Carlo Study. *J. Chem. Phys.* **1997**, *106*, 2865−2880.
(51) Radhakrishnan, R.; Gubbins, K. E. Free Energy Studies of Freezing in Slit Pores: an Order-Parameter Approach Using Monte Carlo Simulation. *Mol. Phys.* **1999**, *96*, 1249−1267.
(52) Radhakrishnan, R.; Gubbins, K. E.; Sliwinska-Bartkowiak, M. Effect of the Fluid-Wall Interaction on Freezing of Confined Fluids: Toward the Development of a Global Phase Diagram. *J. Chem. Phys.* **2000**, *112*, 11048−11057.